Applied Catalysis B: Environmental 117–118 (2012) 148–155

Contents lists available at SciVerse ScienceDirect

Applied Catalysis B: Environmental

journal homepage: www.elsevier.com/locate/apcatb

A novel class of heterojunction photocatalysts with highly enhanced visible light photocatalytic performances: yBiO(Cl_xBr_{1-x})–$(1-y)$ bismuth oxide hydrate

Sanaa Shenawi-Khalil[a,*], Vladimir Uvarov[b], Sveta Fronton[a], Inna Popov[b], Yoel Sasson[a]

[a] Casali Institute of Applied Chemistry, the Institute of Chemistry, the Hebrew University of Jerusalem, Jerusalem 91904, Israel
[b] The Unit for Nanoscopic Characterization, the Center for Nanoscience and Nanotechnology, the Hebrew University of Jerusalem, Jerusalem 91904, Israel

ARTICLE INFO

Article history:
Received 4 December 2011
Received in revised form 5 January 2012
Accepted 9 January 2012
Available online 18 January 2012

Keywords:
Visible light photocatalysis
Heterojunction
Bismuth oxyhydrate
Bismuth hydrate oxide
Bismuth oxyhalide

ABSTRACT

A novel class of heterojunctioned bismuth oxyhalide photocatalysts yBiO(Cl_xBr_{1-x})–$(1-y)$BHO (bismuth oxide hydrate) has been prepared by a simple hydrothermal method. The new materials are highly efficient under visible light irradiation ($\lambda \geq 420$ nm) for the degradation of Rhodamine B (RhB), Acetophenone (AP) and photooxidation of iodide. Even though BHO shows very low photocatalytic efficiency, its combination with BiO($Cl_{0.5}Br_{0.5}$) provides exceptional high photocatalytic activity due to more effective photo-excited electron–hole separation by the heterojunction semiconductor. The relationship between BHO amounts and the photocatalytic activities was investigated. Compared to Degussa P25 the composite with $x = 0.5$ and $y = 0.9$ demonstrated 14.6 times higher activity in removing aqueous RhB under visible light irradiation. The possible photodegradation mechanism was studied by the examination of different active species through adding appropriate scavengers. Furthermore, the photogenerated charge transfer process was proposed based on the bands positions of BiO($Cl_{0.5}Br_{0.5}$) and BHO. After five cycles, the catalyst did not exhibit any significant loss of photocatalytic activity, confirming the photocatalyst is essentially stable. The excellent activity and photostability reveal that yBiO(Cl_xBr_{1-x})–$(1-y)$BHO is a promising visible-light-responsive photocatalyst.

© 2012 Elsevier B.V. All rights reserved.

1. Introduction

In the last few decades water pollution has become a pressing issue worldwide. Clean water is an ever-growing concern these days as various pollutants are constantly finding their way into our water resources. Since numerous organic compounds are resistant to conventional chemical and biological treatment, other methods are being studied as an alternative to biological and classical physico-chemical processes [1]. Among others, semiconductor-based photocatalysis is attracting extensive interest as a kind of "green" technology for degrading toxic pollutants [2]. The main advantage of photocatalysis is that the contaminants could be completely degraded to CO_2, H_2O and other inorganic constituents with solar energy, leaving no waste for second disposal. TiO_2, as the most researched photocatalyst, has a large band gap of 3.2 eV, which limits its effective application of solar energy [3]. This limitation drove scientists to search for modifications and develop new photocatalysts which better exploit the sun's energy.

Bismuth oxyhalides have recently been found to be effectual photocatalysts under UV or visible-light illumination due to their unique layered structure, high activity and high photocorrosion stability [4–9]. It is believed that the formed internal electric fields between the slabs are beneficial to induce the efficient separation of the photogenerated electron–hole pairs and then improving the photocatalytic activity. BiOCl was the first oxyhalide to be used as photocatalyst [5]. The gap of BiOCl ($E_g \sim 3.5$ eV) is wider than that of TiO_2 [7]. Nonetheless, Zhang et al. revealed that BiOCl prepared by a hydrolysis method of Bi_2O_3 in excess HCl, exhibited higher performance on photocatalytic degradation of MO (methyl orange) than Degussa's P25 after three cycles under UV light irradiation [4]. BiOBr, on the other hand, has visible-light response and could act as a good photocatalyst and solar-energy-conversion material [10]. In previous work [11] we showed that a solid solution of BiOCl and BiOBr is possible and could significantly improve the photocatalytic performance under visible light irradiation compared to the individual catalysts. It is well known that formation of a heterojunction between semiconductors with matching energy band potentials is an effective strategy to attain higher photocatalytic activity under visible light conditions. Composite semiconductors can significantly reduce the recombination and speed up the separation rate of photogenerated charge carriers. The fabrication of heterostructures semiconductors concerned BiOX (X = Cl, Br, I) with matching band potentials has be turned out to be an attractive approach for the enhancement of pure BiOX, and several examples such as, BiOCl–Bi_2O_3 [12], BiOCl–WO_3 [13] BiOI–Bi_2O_3 [14], $NaBiO_3$–BiOCl

* Corresponding author. Fax: +972 2 6528250.
E-mail address: shenawi.sanaa@gmail.com (S. Shenawi-Khalil).

0926-3373/$ – see front matter © 2012 Elsevier B.V. All rights reserved.
doi:10.1016/j.apcatb.2012.01.011

[15], AgI–BiOI [16], BiOI–TiO_2 [17], Fe_3O_4–BiOCl [18], have been reported and demonstrated the enhanced photocatalytic activity.

Very recently, we developed an interesting composite between BiOCl and bismuth oxide hydrate (hereafter-BHO) [19]. This heterojunction provided exceptional photocatalytic activity in decomposing RhB under visible light irradiation. Motivated by this work, and other impressive studies on heterostructures of bismuth oxyhalide, we turn out to be interested in the heterojunction between $BiO(Cl_{0.5}Br_{0.5})$ and BHO.

Herein, we describe a novel heterostructured photocatalyst with excellent photocatalytic performance in decomposition typical toxic organics such as, RhB, AP and photooxidation of potassium iodide (KI) under visible light irradiation. The role of BHO and the mechanism of enhanced photocatalytic activity were investigated. To the best of our knowledge, coupling of bismuth mixed halide phases with another semiconductor was not reported before. Therefore, this study offers a new class of highly efficient and promising heterojunctioned photocatalysts for degradation of organic pollutants. This approach of coupling between $BiO(Cl_xBr_{1-x})$ and BHO could be further extended for the synthesis of similar heterostructures with other bismuth mixed halides phases.

2. Experimental

2.1. Synthesis

The powders of the new photocatalysts were synthesized by a simple hydrothermal method followed by acidic hydrolysis. All the reagents were used as received without further purification. The process flow chart for the preparation of the yBiO(Cl_xBr_{1-x})–$(1-y)$BHO heterojunctioned photocatalysts is shown in Fig. S1 (see Supplementary material).

Synthesis of bismuth hydrate oxide ($Bi(OH)_3$): $Bi(NO_3)_3{\cdot}5H_2O$ (99.0%) (10 mmol) was mixed with distilled water (40 mL) and stirred at room temperature for 5 min. Subsequently, NH_4OH (30.0%) (17 mL) was added dropwise. The suspension solution was poured into a stainless steel Teflon-lined autoclave for the hydrothermal treatment. The autoclave was sealed, heated up to 150 °C and held for 12 h, and then cooled to room temperature naturally. The final solid of $Bi(OH)_3$ (2.5 g) was separated by filtration, washed thoroughly with water and dried at air for 24 h.

In order to introduce a coupling between BHO and $Bi(OCl_xBr_{1-x})$, a partial hydrolysis of BHO phase using a specific concentrations of hydrohalic acids (HX, X = Cl and Br) was performed as detailed below.

Synthesis of the heterostructure yBiO(Cl_xBr_{1-x})–$(1-y)$BHO: $Bi(OH)_3$ (2.37 g) was mixed with 150 mL distilled water containing adjusted amounts of HCl and HBr at a ambient conditions for 10 min. The solid was separated by filtration, washed thoroughly with water, and dried at air for 24 h to give yBiO(Cl_xBr_{1-x})–$(1-y)$BHO composite (2.05 g). Typically, when the concentration of each acid was 0.075 M, the percentages of $BiO(Cl_xBr_{1-x})$ to BHO phases were 90/10 (hereafter – $BiO(Cl_{0.5}Br_{0.5})$–BHO (90/10)).

The occurring chemical reactions can be written down as:

$$Bi(NO_3)_3 \cdot 5H_2O + 3NH_4OH \xrightarrow{150\,^\circ C,\,12\,h} Bi(OH)_3 + 3NH_4NO_3 + 5H_2O \quad (1)$$

$$Bi(OH)_3 + xHCL + (1-x)HBr \xrightarrow{25\,^\circ C,\,10\,min} BiO(Cl_xBr_{1-x}) + 2H_2O \quad (2)$$

Thus processing of originally formed $Bi(OH)_3$ particles by acids (HCl and HBr) has led to heterojunction structure formation. Particulate TiO_2 (particle diameter 30 nm, surface area 50 $m^2\,g^{-1}$, product name P25) is commercially available from Degussa Corp. and it was used as a reference photocatalyst.

Synthesis of $BiO(Cl_xBr_{1-x})$: The solid solutions of $BiO(Cl_xBr_{1-x})$ were prepared as reported in Ref. [11]. Specifically, $BiO(Cl_{0.5}Br_{0.5})$ was synthesized as follows: $Bi(OH)_3$ (2.37 g) was mixed with 150 mL distilled water, containing excess (≥0.1 M) of HCl and HBr with the same molar ratio at ambient conditions for 30 min. The solid product was separated by filtration, washed thoroughly with water and air-dried for 24 h to afford the product (2.12 g).

2.2. Photocatalytic activity test

Photocatalytic activities of the new photocatalyst powders were evaluated using two types of reactions: the photo-bleaching of water organic pollutants: Rhodamine B (RhB) and Acetophenone (AP) and the photocatalytic oxidation of iodide, under irradiation at wavelengths range of 385–740 nm and visible light irradiation at $\lambda \geq 420$ nm. Experiments were carried out in a 250 mL cylindrical-shaped-glass reactor at room temperature in air and at neutral pH conditions. A suspension of 100 mg photocatalyst and 200 mL aqueous solution of RhB (15 ppm) or AP (120 ppm) or KI (25 mmol L^{-1}) was magnetically stirred for 2 h or more before irradiation to establish an adsorption–desorption equilibrium. The reactor was then irradiated by a 300 W Xe arc lamp (Max-302, Asahi spectra). Power consumption of Max-302 is 500VA. The emission spectrum is shown in Fig. S2 (see Supplementary material). The lamp is equipped with visible mirror (Fig. S2b, Supplementary material). This unit consists of several multicoated filters to block unwanted energy from Xenon lamp and only desired throughput (385–740 nm) is obtainable. For visible light experiments a 420 nm cutoff filter was used. The light intensity was fixed on 70 mW/cm^2 when the reactor was placed 10 cm away from the light's source mirror. At specific time intervals, 4 mL suspensions were sampled and centrifugated at 6000 rpm for 10 min to remove the photocatalyst powder. The concentration of remnant RhB or AP in solution after irradiation was analyzed with a UV–vis spectrophotometer (Varian EL-03097225) by recording the variations of the absorption band maximum at λ = 554 nm and λ = 235 nm respectively. The degradation efficiency (DE) of each catalyst was computed using the following equation:

$$DE = 100\% \times \frac{C_0 - C}{C_0} \quad (3)$$

where C is the concentration of RhB (or AP) at the time interval t and C_0 is the concentration after the adsorption equilibrium is reached before irradiation.

The tri-iodide production was also spectrophotochemically monitored by measuring the absorbance at 352 nm.

RhB was chosen as a typical model compound since dyes are important water pollutants. Most of the dyes are resistant to biodegradation and direct photolysis, and many N-containing dyes such as RhB undergo natural reductive anaerobic degradation to yield potentially carcinogenic aromatic amines [20]. Acetophenone is a common colorless water pollutant. To differentiate from the photodecomposition of organics which is categorized as a downhill reaction and is thermodynamically preferable, we also studied the photooxidation of KI which is an uphill reaction (+51 kJ/mol). Production of energy-carrying materials through thermodynamically uphill reactions is an important objective of solar energy conversion and storage.

The Langmuir adsorption constants were calculated by dark adsorption experiments of RhB. 100 mL of aqueous RhB solutions of various initial concentrations (C_0 = 6 ppm, 9 ppm, 15 ppm and 18 ppm) and 50 mg catalyst were stirred in a closed glass bottle, in ambient temperature, for approximately 24 h. All bottles were covered by aluminum foil to avoid light illumination. The suspensions

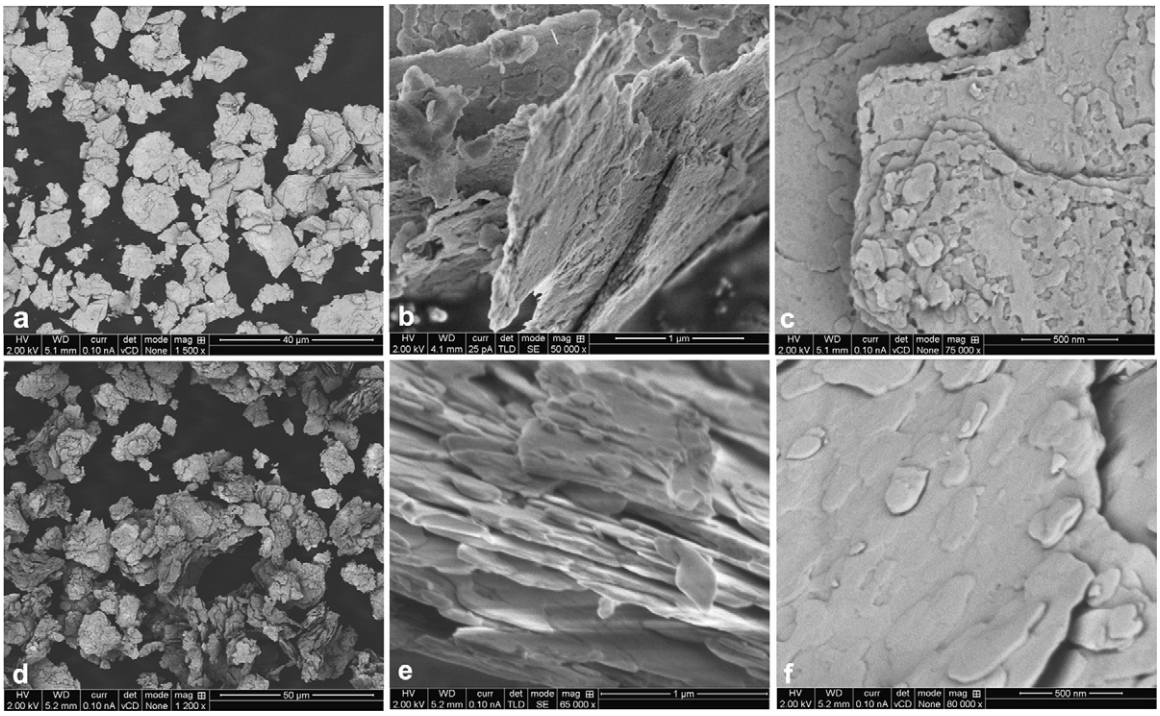

Fig. 1. SEM images acquired from dry powders of as-synthesized yBiO($Cl_{0.5}Br_{0.5}$)–(1 − y)BHO (y = 0.45) (a–c) and BiO($Cl_{0.5}Br_{0.5}$)/BHO (90/10) mechanical mixture (d–f).

were then centrifuged to remove the photocatalyst powder. The concentration of remnant RhB in solution after adsorption (which is the equilibrium concentration C_{eq}) was analyzed with a UV–vis spectrophotometer (Varian EL-03097225) by recording the variations of the absorption band maximum at λ = 554 nm.

The data collected was fitted to Langmuir linear equation (Eq. (4)):

$$\frac{1}{N} = \left(\frac{1}{K_L \cdot N_{max}}\right) \cdot \frac{1}{C_{eq}} + \frac{1}{N_{max}} \quad (4)$$

where K_L [l mmol^{-1}] is the Langmuir adsorption constant, N_{max} [mmol g^{-1}] is the maximal amount of adsorption possible, and N is the amount of adsorption in the experiment. N was calculated as following:

$$N = \frac{V(C_0 - C_{eq})}{M} \quad (5)$$

where V (solution volume) is 0.1 l and M (catalyst mass) is 0.05 g.

In experiments requiring radical scavengers, excess amount of 1.0 mM benzoquinone (BQ) or $KBrO_3$ and 500 mM isopropanol (IPA) were introduced to RhB solution before the addition of catalyst.

Fluorescence spectra of 2-hydroxyterephthalic acid were measured on Varian Cary Eclipsed fluorescence spestrophotometer-0010075200. The OH• radical trapping experiments were carried out using the following procedure: terephthalic acid (TA) (16.6 mg) was first dissolved in 200 mL dilute NaOH solution (2×10^{-3} M), followed by addition of 100 mg photocatalysts. The suspension was irradiated by 300 W Xenon lamp at wavelengths range of 385–740 nm for 60 min. The fluorescence emission spectrum of the solution was measured every 10 min during illumination.

Recycling experiments were performed as follows: after each cycle the catalyst was separated by centrifugation, washed thoroughly with distilled water and added to a fresh AP (120 ppm) aqueous solution.

2.3. Material characterization

Morphological observations and identification of the chemical composition were performed with the Extra High Resolution Scanning Electron Microscopy (XHR SEM) Magellan^{TM} 400L (FEI Company, Netherland) equipped with large area EDS silicon drift detector Oxford X-Max (Oxford Instruments, UK). Pure β-Bi_2O_3 (Aldrich) was used for checking the accuracy of standardless quantification of EDS results. For quantitative analysis the EDS spectra were acquired at 20 kV accelerating voltage.

XRD measurements were performed on D8 Advance diffractometer (Bruker AXS, Karlsruhe, Germany) with a goniometer radius 217.5 mm, Göbel Mirror parallel-beam optics. XRD patterns from 5° to 75° 2θ were recorded at room temperature using Cu Kα radiation (λ = 0.15418 nm) with following measurement conditions: tube voltage of 40 kV, tube current of 40 mA, step scan mode with a step size 0.02° 2θ and counting time of 1 s per step. The instrumental broadening was determined using LaB_6 powder (NIST-660a).

3. Results and discussion

3.1. Structural morphological and chemical characterization of the synthetic products

Fig. 1 shows images acquired from dry as-synthesized yBiO(Cl_xBr_{1-x})–(1 − y)BHO (x = 0.5 and y = 0.45) powder and a mechanical mixture of BiO($Cl_{0.5}Br_{0.5}$)/BHO (90/10). As is seen in Fig. 1, particles of both powders have very similar plate-like morphology with the plates having lateral dimensions of tens of microns. Being imaged in back-scattered electrons (Fig. 1a, c, d and f) both powders exhibit uniform contrast at wide magnification range (~1000× (Fig. 1a and d)–75,000× (Fig. 1c and f)) that indicates uniform chemical composition within the whole plate as well as within its small structural constituents of less about 100 nm size. Imaging in secondary electrons (Fig. 1b and e) revealed topographical details of the observed plate-like morphology. Although

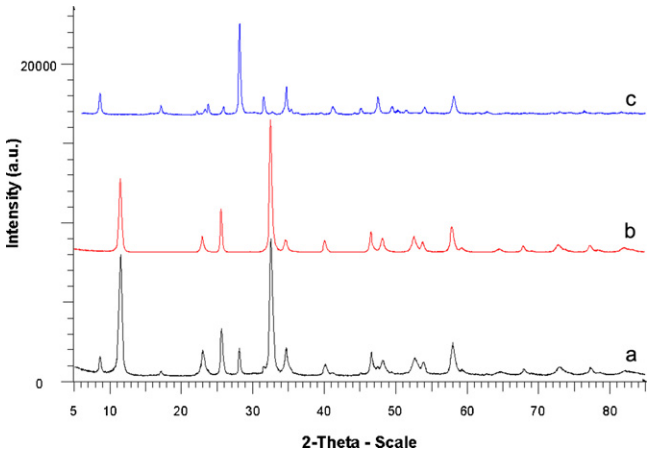

Fig. 2. XRD patterns acquired from as-synthesized (a) yBiO($Cl_{0.5}Br_{0.5}$)–$(1-y)$BHO sample (with $y = 0.9$), (b) pure BiO($Cl_{0.5}Br_{0.5}$) and (c) pure BHO.

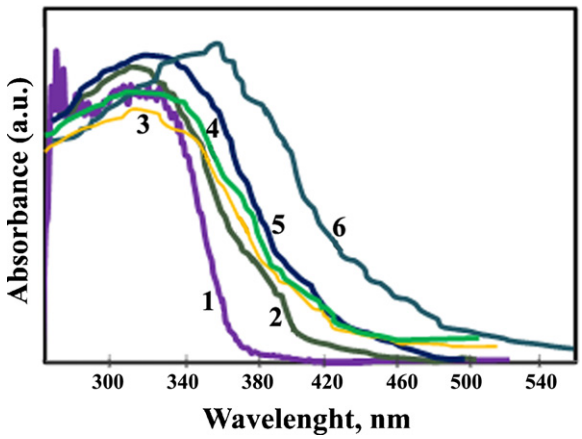

Fig. 3. Diffuse reflectance spectra of (1) BiOCl; (2) 0.8BiOCl–0.2BHO; (3) BiO($Cl_{0.5}Br_{0.5}$); (4) BiO($Cl_{0.5}Br_{0.5}$)–BHO (90/10); (5) BHO and (6) BiOBr.

the lateral dimensions of plates were about tens of microns, their thickness was roughly three orders of magnitude smaller at the range of tens of nanometers. The thickness was non-uniform across a plate so that the plates exhibited rather multi-layered structure with varying number of thin layers within each single plate. Plates of a mechanical mixture appear smoother than those in the as-synthesized powder. This correlates well with the differences in their surface area found with BET analysis (see Table 3).

Fig. 2a shows the XRD patterns acquired from as-synthesized yBiO(Cl_xBr_{1-x})–$(1-y)$BHO sample (with $y = 0.9$ and $x = 0.5$). Analysis of the XRD pattern revealed that the sample is a mixture of two crystalline phases. One of these phases was identified as the BiO($Cl_{0.5}Br_{0.5}$) (unit cell parameters $a = b = 3.89$ Å, $c = 7.73$ Å, $P4/nmm$ (No. 129) space group) [11] and the second one was identified as BHO (unit cell parameters $a = b = 5.67$ Å, $c = 10.35$ Å, $P4/mmm$ (No. 123) space group) [19]. Fig. 2b and c shows XRD patterns obtained from pure BiO($Cl_{0.5}Br_{0.5}$) and pure BHO phases (for comparison). It should be noted that very similar XRD pattern was presented in Fig. 5a in [21] (authors have specified that XRD pattern was obtained from a pure bismuth hydroxide purchased from Shepherd Chemicals (Norwood, OH)). Usually, $Bi(OH)_3$ is considered as an amorphous material. Notable that back in 1931 Huttig et al. have published an article [22], in which they had indicated that the compound $Bi_2O_3 \cdot 3H_2O = Bi(OH)_3$ does exist and had reported results of XRD investigation they made on the synthesized material. They named this material bismuth oxide hydrate and according to Frondel [23] their data suggest that this compound is not trihydrate, specifically it is a dihydrate. Therefore, in our opinion its formula should be written as $[Bi_2O_2]^{2+}(OH)_2^- \cdot 2H_2O$. Such presentation clarifies close relation of BHO to a family of layered bismuth oxyhalides. The composition of BiO(Cl_xBr_{1-x}) was calculated as described in our recent work [11] using value of the c-parameter obtained from XRD data via $x = 10.966 - 1.354c$ (x is content of chlorine). The ratio between BiO(Cl_xBr_{1-x}) and BHO phases was estimated with using the quantitative XRD analysis based on normalized reference intensity ratios (RIR) method [24]. This method is realized in the EVA software (Bruker AXS) and content of phases is calculated using the following equation:

$$C_i = 100\% \times \left(\frac{I_i K_i}{\sum_{i=1}^{n} I_i K_i} \right) \quad (6)$$

where n is number of phases in the specimen, C_i is percentage of i-th phase, I_i is intensity of i-th phase and K_i is corundum coefficient of i-th phase.

Taking into account that BiOCl and BiOBr phases have the same crystal structure and their K_i values are published in JCPDF database, we can calculate K_i value for a phase with any x value using the formula $K_i = 14.5 - 4.6x$. Further we can calculate K value for BHO phase using Eq. (6) and I_i values measured on XRD pattern acquired from a two-phase artificial mixture with known composition. This work has been performed, and we obtained the K value for BiO($Cl_{0.5}Br_{0.5}$) equal to 12.2 and the K value for BHO equal to 9.9. The calculated K_i values were used at semiquantitative XRD analysis of synthesized specimens. Crystallite size of both phases as-estimated from the XRD data with using Scherrer equation (as described in [25]) was of the same order of magnitude (about 35–45 nm) that along with the identical plate-type morphology supports suggestion about atomic scale phase mixing or even possibility for intergrowth.

3.2. Photophysical properties of the new photocatalysts

UV–vis diffuse reflectance spectra (DRS) of BiOCl, BiOBr, BiO($Cl_{0.5}Br_{0.5}$), BHO, 0.8BiOCl–0.2BHO and the new heterojunction photocatalyst, BiO($Cl_{0.5}Br_{0.5}$)–BHO (90/10), are shown in Fig. 3. The band gaps (E_g) of the samples were estimated from the onsets of the absorption edges using the formula $\lambda_g = 1239/E_g$, where λ_g is the band gap wavelength [26]. In our previous work [11] on the pure mixed halides phases it was confirmed that for all samples the band gap is indirect. Based on DRS results the estimated band gaps are 3.31, 2.95, 2.91, 2.89, 2.81 and 2.58 eV for BiOCl, 0.8BiOCl–0.2BHO, BiO($Cl_{0.5}Br_{0.5}$), BiO($Cl_{0.5}Br_{0.5}$)–BHO (90/10), BHO and BiOBr respectively. The band gap of the new composite lies, as expected, between the two values of the side members BiO($Cl_{0.5}Br_{0.5}$) and BHO, and is closer to the band gap of the mixed halide phase.

3.3. Appraisal of the photocatalytic activity

The photocatalytic properties of the new composite materials were studied under irradiation at wavelengths range of 385–740 nm, and visible light ($\lambda \geq 420$ nm) conditions using three different tests: the degradation of RhB, AP and the photooxidation of KI.

3.3.1. Rhodamine B photodegradation

To evaluate the photocatalytic activity of the as-prepared yBiO(Cl_xBr_{1-x})–$(1-y)$BHO photocatalysts, the photodegradation of the well-known organic azo-dye Rhodamine B (RhB), a typical pollutant in the textile industry, was investigated in water under different irradiations. Its characteristic absorption at about 554 nm has been used to monitor the photocatalytic degradation process.

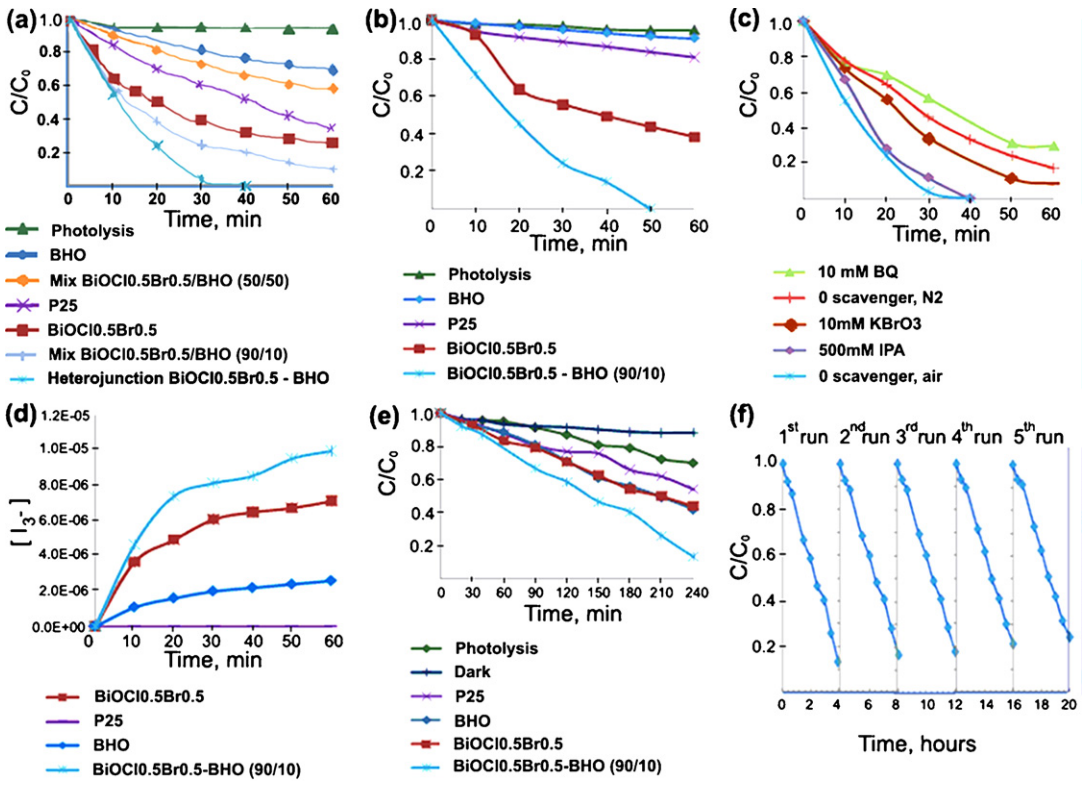

Fig. 4. Comparison of the photocatalytic degradation of RhB (15 ppm) in presence of different photocatalysts and photolysis of RhB under (a) irradiation at wavelengths range of (385–740 nm); (b) under visible light irradiation ($\lambda \geq 420$ nm); (c) effects of BrO_3^-, BQ, IPA and N_2 purging on degradation of RhB over BiO($Cl_{0.5}Br_{0.5}$)–BHO (90/10); (d) photooxidation of KI (25 mmol L^{-1}) over different photocatalysts under visible light ($\lambda \geq 420$ nm) irradiation; (e) photocatalytic degradation of AP (120 ppm) over different photocatalysts under visible light ($\lambda \geq 420$ nm) irradiation; (f) cycling runs in photocatalytic degradation of AP in presence of BiO($Cl_{0.5}Br_{0.5}$)–BHO (90/10).

Fig. 4a and b presents the variation of RhB concentration (C/C_0) as the function of irradiation time for experiments carried out under irradiation at wavelengths range of 385–740 nm and visible light ($\lambda \geq 420$ nm) conditions respectively. For comparison, the photocatalytic activity of Degussa's P25, and the direct non-catalytic photolysis of RhB were tested under the same conditions.

The results show that RhB is fairly stable under visible light irradiation, where the RhB degradation by the photolysis mechanism is not observable. Whereas, a rapid decrease in the RhB concentration is revealed when the new heterojunctioned photocatalyst with the composition BiO($Cl_{0.5}Br_{0.5}$)–BHO (90/10) is applied, which demonstrates that this catalyst exhibits excellent photocatalytic activity. The degradation efficiency of RhB reaches its maxima (100%) within only 40 min of irradiation at wavelengths range of 385–740 nm, compared to DE of 65.2% after 1 h for P25.

To demonstrate the favorable photocatalytic activity induced by the synergistic effect of the coupled BiO($Cl_{0.5}Br_{0.5}$)–BHO (90/10), its activity for the degradation of RhB was compared with the pure components, i.e. BiO($Cl_{0.5}Br_{0.5}$) and BHO, and their physical mixtures with weight ratios of 9:1 and 1:1 (Fig. 4a). The new composite (with $x = 0.5$ and $y = 0.9$) is superior to the pure BiO($Cl_{0.5}Br_{0.5}$) and BHO in promoting the decomposition of RhB under irradiation at wavelengths range of 385–740 nm or at $\lambda \geq 420$ nm. BHO by itself has a very small photocatalytic activity attributed to favored e–h recombination processes, derived, most likely, from large number of defects sites. The formation of heterojunction between BHO and bismuth oxyhalide phase can minimize those undesired processes (as shown in Section 3.3.2.2) and considerably promotes the photodegradation pathway. However, a simple combination of the pure components is much less effective in promoting the photodecomposition of RhB.

Visible-light-induced photocatalysis was confirmed by measuring the RhB degradation under irradiation with ($\lambda \geq 420$ nm) as shown in Fig. 4b. The order of reactivity of all samples was similar to the order observed under irradiation at wavelengths range of 385–740 nm. Notably, the absolute values of DE were slightly smaller for BiO($Cl_{0.5}Br_{0.5}$) and BiO($Cl_{0.5}Br_{0.5}$)–BHO (90/10) under visible light irradiation. However, P25 under visible light exhibited extremely low photodegradation efficiency (19.7% after 60 min). Compared with our previous work [19] on the heterojunction between BHO and BiOCl, the present composition is much more reactive due to a better e–h separation, derived directly from the favored relative positions of VB and CB edges as will be shown is Section 3.3.2.2.

The degradation of RhB under visible-light irradiation may proceed via three possible mechanisms, including a photocatalytic mechanism, a dye photosensitization mechanism and a photolysis mechanism. As displays in Fig. 4b, the degradation of RhB without any catalyst under visible light irradiation is negligible, suggesting that RhB cannot be degraded by the photolysis route. TiO_2, is used as a typical catalyst to study the photosensitization mechanisms [6,27]. However, in our experiment it shows very low photocatalytic performance under visible light irradiation, which confirms that, the degradation of RhB in the present study is initiated, mainly, by the photocatalytic mechanism.

yBiO(Cl_xBr_{1-x})–$(1-y)$BHO phases were prepared using different amounts of HCl and HBr, so that different x and y values were observed. This is in order to find out the best combination, i.e. the optimal molar ratio between BiO(Cl_xBr_{1-x}) and BHO phases, which leads to the highest photocatalytic performance. Furthermore, the

Table 1
DE(%) and the pseudo-first-order rate constants for the degradation of RhB under different irradiation conditions over yBiO(Cl_xBr_{1-x})–(1 − y)BHO photocatalysts.

x value (y = 0.9)	k (min^{-1}) λ = 385–740 nm	k (min^{-1}) λ ≥ 420 nm	DE (%) after 1 h λ = 385–740 nm	DE (%) after 1 h λ ≥ 420 nm
0.2	0.0244	0.0128	76.0	45
0.5	0.1044	0.0498	100	100
0.7	0.0288	0.0132	81.5	48

Table 2
DE(%) and the pseudo-first-order rate constants for the degradation of RhB under different irradiation conditions over yBiO($Cl_{0.5}Br_{0.5}$)–(1 − y)BHO photocatalysts.

y value (x = 0.5)	k (min^{-1}) λ = 385–740 nm	k (min^{-1}) λ ≥ 420 nm	DE (%) after 1 h λ = 385–740 nm	DE (%) after 1 h λ ≥ 420 nm
0	0.0061	0.0017	30.8	9.65
0.05	0.0269	0.0146	80.4	59.05
0.18	0.0501	0.0144	98.0	59.16
0.45	0.0205	0.0124	97.5	52.49
0.80	0.0422	0.0161	92.3	61.13
0.90	0.1044	0.0498	100	100
0.98	0.0316	0.0173	85.4	63.13
1.0	0.0224	0.0167	72.4	62.07
P25	0.0174	0.0034	65.2	19.67

kinetics of RhB degradation was studied quantitatively by applying the pseudo-first-order model as expressed by Eq. (7):

$$\ln\left(\frac{C_0}{C}\right) = kt \quad (7)$$

where k is the pseudo-first-order rate constant.

The DE of the different composites and the rate constants are listed in Tables 1 and 2.

As seen from Tables 1 and 2, The composite with x = 0.5 and y = 0.9 exhibits the highest photocatalytic activity in decomposing RhB. Concerning the pure mixed halides phases, BiO(Cl_xBr_{1-x}) (x = 0.0–1.0), it was verified in our previous work [11] that the phase with x = 0.5 has the best performance, since at this point the competition between light absorption and the photooxidation power reaches its optimal value. Conceivably, for the same reason its combination with BHO is favored over other compositions with $x \neq 0.5$.

Noticeably, changing the molar ratios between BiO($Cl_{0.5}Br_{0.5}$) and BHO has decisive effect on the degradation rate and efficiency. Still, there is no linear correlation between the increase (or decrease) in y values and the photocatalytic activity. Furthermore, it is obvious that the new heterostructure is active over a wide range of y values.

The Brunauer–Emmett–Teller surface area (A_{BET}) has been used to characterize the surface areas of the samples. The adsorption percentages of RhB on the photocatalysts in the dark for 60 min were also examined. Langmuir adsorption constants (K_L) were calculated according to Section 2.2. The results from those experiments are represented in Table 3. No correlation has been found between the surface areas with either the photocatalytic activities or K_L (and % adsorption), suggesting that the surface area of the photocatalysts does not play a crucial role on the photocatalytic process, and that the adsorption of the dye depends on other factors. BHO showed the smallest surface area. On the other hand, after its coupling with the mixed halide phase an increase in the A_{BET} is observed. Surprisingly, the samples with y = 0.18 and 0.45 exhibited a very large surface area compared to other samples, but not the highest photocatalytic performances. However this result was easily explained after the SEM analysis (see Fig. 1b and c). Usually clean plate-like particles of synthesized material look strongly corroded and this has increased the surface area. % adsorption of RhB is approximately the same for all yBiO($Cl_{0.5}Br_{0.5}$)–(1 − y)BHO catalysts and range from 28 to 40%, except for samples with y = 0.9 and 0.18 where higher values are observed. Evidently, the preadsorption of the dye is an important factor for the photocatalytic degradation, especially in our case where the photodecomposition mechanism is not proceeding via the OH• radical (as discussed in Section 3.3.2). However, there are other factors that are believed to play an essential role in the photocatalytic process, such as the capability of absorbing the incident light, e–h separation, and others.

Table 3
Brunauer–Emmett–Teller surface area (A_{BET}), % adsorption of RhB at dark and Langmuir constants (K_L).

y value (calculated)	K_L	% Adsorption	A_{BET} (m^2 g^{-1})
0.00	66.6	6.80	1.35
0.05	301.0	39.80	1.82
0.18	469.6	46.50	11.00
0.45	207.3	37.09	11.50
0.80	161.0	26.40	2.105
0.90	579.3	55.76	5.75
0.98	188.0	28.50	3.25
1.00	178.0	23.60	4.02
P25	76.27	6.85	50.00

3.3.2. *The mechanism of photodegradation of RhB under irradiation in the range of 385–740 nm*

3.3.2.1. Effect of scavengers and N_2 purging. The effect of some radical scavengers and N_2 purging on the degradation of RhB under irradiation at wavelengths range of 385–740 nm over yBiO($Cl_{0.5}Br_{0.5}$)–(1 − y)BHO photocatalyst was examined in an attempt to better understand the reaction mechanism. To detect the presence of OH• radical, we used terephthalic acid (TA) as a fluorescent probe. OH• radical is known to be trapped by TA to produce the fluorescent 2-hydroxyterephthalic acid [28]. For comparison, the TiO_2 system was also monitored under the same conditions. The results are shown in Fig. S3 (see Supplementary material). There were no observable peaks when the bismuth derived suspensions were irradiated. However, in the case of TiO_2 (Fig. S3a in Supplementary material) gradual increase in the fluorescence intensity at ca. 425 nm was observed with increasing illumination time. The generated spectrum has the identical shape and maximum wavelengths with that of 2-hydroxyterephthalic acid indicating the OH• radical was indeed formed. In another experiment, it was found that the addition of 2-propanol, another well known scavenger of OH• radicals [29], into the photoreaction system did not cause any apparent changes in the degradation

rate of RhB as shown in Fig. 4c. However, a sharp decrease in the photodegradation efficiency was observed when P25 was used (see Fig. S4 in Supplementary material).

In a valence band of Bi^{3+}, holes formed by photoexcitation are regarded as Bi^{5+} [30]. The standard redox potential of Bi^{V}/Bi^{III} is more negative than of $OH^{\bullet}/OH^{-}$ [31]. Therefore, photogenerated holes on the surface of yBiO($Cl_{0.5}Br_{0.5}$)–$(1-y)$BHO are not expected to react with OH^{-}/H_2O to form $OH^{\bullet}$, suggesting that the decomposition of RhB and AP could be attributed to a direct reaction with the photogenerated holes or with superoxide radical (generated by the excited electron) or both species. Therefore, the RhB molecules to be degraded should be adsorbed preferentially on the surface of the photocatalyst. As shown from Table 3, the highest adsorption percentage of RhB was reached over BiO($Cl_{0.5}Br_{0.5}$)–BHO (90/10), which consequently exhibited the highest photocatalytic reactivity. Using P25, the dominant species for the degradation of RhB are the $OH^{\bullet}$ radicals, thus, the adsorption of the dye is not critical.

To investigate the role of superoxide radical, N_2 purging experiment was conducted compared with air-equilibrated conditions. It can be seen from Fig. 4c that considerable decrease in the decomposition efficiency was obtained under N_2 purging. This result suggests that dissolved oxygen is essential to RhB degradation. An additional test was performed to further explore the role of superoxide radical. Excess of bromate ($KBrO_3$), which is a strong oxidant [32,33] was added to the reaction system. This oxidant proved to be an effective electron acceptor replacing oxygen, thus suppressing the production of superoxide radical and accelerate the separation of e_{cb}^{-}–h_{vb}^{+} in the photocatalyst. As can be seen in Fig. 4c the addition of $KBrO_3$ has a negative effect on the degradation efficacy of RhB, confirming that the superoxide radical is indeed an active species in the RhB photodegradation process over the heterojunctioned catalyst. However, the large excess of bromate could not terminate the degradation of RhB. This clearly suggests that other active species are involved in the decomposition and those are, most likely, the holes in the valence band of BHO. This conclusion was supported by third test, in which BQ was used as a quencher of $O_2^{\bullet-}$. The addition of BQ, as seen from Fig. 4c, could greatly decrease the photocatalytic efficiency of RhB but could not completely stop the reaction, again supporting the above conclusions.

3.3.2.2. Band gap structures and possible degradation mechanism. The determination of CB and VB edge electrochemical potentials of a semiconductor is essential in order to understand the photodegradation mechanism of pollutants. The bands edge positions of yBiO($Cl_{0.5}Br_{0.5}$)–$(1-y)$BHO (90/10) photocatalyst were theoretically predicted using atom's Mulliken electronegativity definition [34]:

$$E_{VB} = \chi - E^{e} + \frac{1}{2E_g} \quad (8)$$

where χ is the electronegativity of the semiconductor, E^{e} is the energy of free electrons on the hydrogen scale (≈4.5 eV), and E_g is the band gap energy of the semiconductor. According to this empirical expression the calculated CB (E_{CB}) and VB (E_{VB}) edge positions for BHO and BiO($Cl_{0.5}Br_{0.5}$) photocatalysts are shown in Fig. 5. It can be seen that VB edge potential of BHO is more positive than the standard redox potential of $OH^{\bullet}/OH^{-}$ (1.99 eV), suggesting that the photo-generated hole is far more oxidative than $OH^{\bullet}$ radical.

In accordance with the band edges values of both BHO and BiO($Cl_{0.5}Br_{0.5}$), the heterojunction designed in this work is schematically represented in Fig. 5. This is a special type of heterojunction since both SCs are activated under visible light irradiation and subsequently generate electrons and holes. The relative positions of the VB and CB bands enable the transfer of electrons as well as transfer of holes between BHO and BiO($Cl_{0.5}Br_{0.5}$). The coupling of those two SCs can help in improving charge separations,

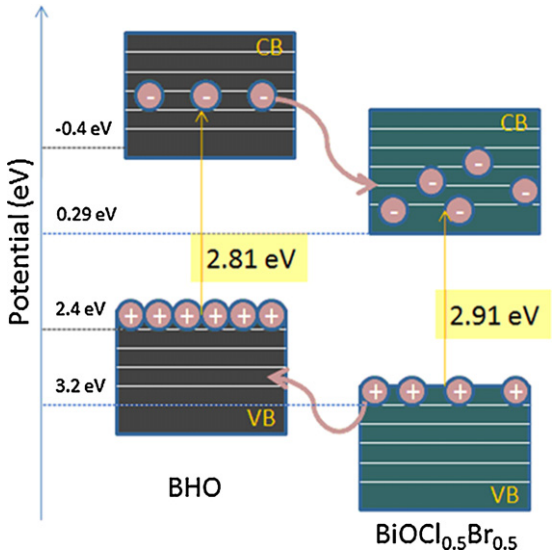

Fig. 5. Schematic diagram for band gap structure and flow of electrons of yBiO($Cl_{0.5}Br_{0.5}$)–$(1-y)$BHO systems during irradiation at $\lambda \geq 420$ nm or in the range of 385–740 nm.

increasing life times of the charge carriers and enhancing the efficiency of the interfacial charge transfer to the adsorbed substrate. The excellent separation of the holes and electrons in the heterojunction of yBiO($Cl_{0.5}Br_{0.5}$)–$(1-y)$BHO and the deep VB of BHO are the main reasons for the exceptional photocatalytic activity of the studied system.

Although yBiO(Cl_xBr_{1-x})–$(1-y)$BHO heterostructure may resemble to some extent, the recently reported yBiOCl–$(1-y)$BHO [19], fundamental differences can be found, which demonstrate the novelties of the present system. The heterojunction between BiO(Cl_xBr_{1-x}) and BHO is favored over the yBiOCl–$(1-y)$BHO heterostructure. Several reasons may account for the higher photocatalytic activity of the present heterostructure. Among others, the most important are the band gap structure and the flow of holes and electrons through the heterojunction. Unlike yBiO(Cl_xBr_{1-x})–$(1-y)$BHO, in yBiOCl–$(1-y)$BHO only BHO can be activated under visible light irradiation. There is no simultaneous migration of electrons and holes through the heterojunction, since the holes in the VB of BHO cannot transfer to the non-excited BiOCl semiconductor. Subsequently, the separation of charge carries is expected to be more efficient in the yBiO(Cl_xBr_{1-x})–$(1-y)$BHO system. Moreover, the effective band gap energy of yBiO(Cl_xBr_{1-x})–$(1-y)$BHO is smaller than that of yBiOCl–$(1-y)$BHO, thus it can utilize the incoming visible light energy more effectively. Accordingly, the more efficient charge separation and energy absorption observed in yBiO(Cl_xBr_{1-x})–$(1-y)$BHO, definitely support the increase of 25% in photocatalytic activity in decomposing RhB under visible light irradiation. Therefore, this study presents a new approach for improving the activity of pure bismuth oxyhalide phases; first by generation of a hybrid semiconductor between two BiOX phases with different halides, such as, BiO(Cl_xBr_{1-x}), BiO(I_xBr_{1-x}) or BiO(Cl_xI_{1-x}), and second by a formation of heterojunction between the mixed halide phase and bismuth oxide.

3.3.3. Photooxidation of KI under visible light irradiation

Fig. 4d presents another set of experiments where the formation of tri-iodide from iodide under visible light irradiation is shown. To the best of our knowledge we are the first to study the photooxidation of KI by bismuth oxyhalides photocatalysts. The potential of a semiconductor to photooxidize iodide to tri-iodide is directly related to its band gap value. In order to oxidize the iodide the

hole should first react with the adsorbed iodide ion to form an iodine atom that can further react with the iodide ion to produce I_2^-. The I_2^- disproportionate to form triiodide and iodide ion [35]. To differentiate from the photosensitization mechanism, in the KI photooxidation the catalyst must be excited. As indicated in Fig. 4d, the oxidation of iodide is negligible with P25 under visible-light ($\lambda \geq 420$ nm). This is because holes cannot be generated under visible light irradiation in TiO_2. Nonetheless, sufficient amounts of tri-iodide were produced when the $BiO(Cl_{0.5}Br_{0.5})$, BHO and $BiO(Cl_{0.5}Br_{0.5})$–BHO (90/10) were used. Similarly to RhB system, the reactivity of the latter was much higher than that of the pure components.

3.3.4. AP degradation under visible light irradiation

For the reason that the competition between photosensitization and photocatalytic processes are taking place during dye degradation under visible light irradiation, the photocatalytic activity of $BiO(Cl_{0.5}Br_{0.5})$–BHO (90/10), $BiO(Cl_{0.5}Br_{0.5})$, BHO and P25 has been monitored using Acetophenone as a probe molecule. AP does not absorb in the visible range, therefore its degradation is evidence of photocatalytic activity under visible light irradiation. Fig. 4e shows the degradation of AP under visible light irradiation. As a comparison, direct photolysis of AP, and a dark reaction are also recorded. Unlike RhB, AP is not very stable under visible light irradiation, with about 30% of AP being decomposed within 4 h of irradiation even in the absence of a catalyst. The adsorption of AP on the catalyst surface was measured under dark conditions. The adsorption–desorption equilibrium was reached after 60 min, with an adsorption of 9.3% of the AP. The sample with $y = 0.9$, $x = 0.5$ is highly effective in accelerating the decomposition of AP under visible light irradiation, significantly increasing the rate of AP decomposition (86.6% within 4 h).

To confirm the stability and reusability of $BiO(Cl_{0.5}Br_{0.5})$–BHO (90/10) photocatalyst, the five circulating runs in the photocatalytic decomposition of AP under visible light irradiation were checked under the same conditions. As shown in Fig. 4f, $BiO(Cl_{0.5}Br_{0.5})$–BHO (90/10) still exhibited effective degradation after five cycles with only 11% decrease in the photocatalytic efficiency. It indicates that the new material is highly stable and does not photocorrode during the photocatalysis of the model pollutant molecules, which is principal for its applications.

4. Conclusions

In a summary, a new class of highly active visible-light photocatalysts $yBiO(Cl_{0.5}Br_{0.5})$–$(1-y)$BHO was synthesized by a simple hydrothermal method under basic conditions. The new heterostructures notably demonstrate a wide composition range in decomposing RhB, and the optimized activity is obtained at $y = 0.9$ and $x = 0.5$. This composite provides unprecedented high efficiency in decomposing RhB, AP and photooxidation of KI under visible light irradiation. The synergetic effect of the coupling between $BiO(Cl_{0.5}Br_{0.5})$ and BHO, which consequently leads to the effective separation of the charge carriers, is the main reason for the induced favorable photocatalytic performances of the heterojunctioned photocatalysts. For the same reason, the present heterostructure demonstrates an increase of 25% in the photocatalytic degradation of RhB compared with $yBiOCl$–$(1-y)$BHO composite. Furthermore, the new material exhibits 14.6 times higher activity in removing aqueous RhB under visible light irradiation than Degussa P25. It was ascertained that the material obtained at simple mechanical mixing of nanosized $BiO(Cl_xBr_{1-x})$ and BHO (at weight ratio of 90/10) powders also possesses photocatalytic properties, which is higher than same for initial phases. Photocatalytic mechanism investigations prove that the degradation of RhB under irradiation at $\lambda \geq 420$ nm or at wavelengths range of 385–740 nm over the as-prepared $BiO(Cl_{0.5}Br_{0.5})$–BHO (90/10) is mainly via the direct hole oxidation mechanism and superoxide oxidation pathways. The recycling experiments indicate that $BiO(Cl_{0.5}Br_{0.5})$–BHO (90/10) has good durable photocatalytic activity and chemical stability. Therefore, this work provides a facile route to the synthesis of a highly active photocatalysts, and sheds some light on the improvement of the photocatalytic properties of bismuth-based oxyhalides by designing the heterojunction.

Appendix A. Supplementary data

Supplementary data associated with this article can be found, in the online version, at doi:10.1016/j.apcatb.2012.01.011.

References

[1] S. Esplugas, J. Giménez, S. Contreras, E. Pascual, M. Rodríguez, Water Res. 36 (2002) 1034–1042.
[2] M.R. Hoffmann, S.T. Martin, W. Choi, D.W. Bahnemann, Chem. Rev. 95 (1995) 69–96.
[3] A.L. Linsebigler, G. Lu, J.T. Yates, Chem. Rev. 95 (1995) 735–758.
[4] K.L. Zhang, C.M. Liu, F.Q. Huang, C. Zheng, W.D. Wang, Appl. Catal. B 68 (2006) 125–129.
[5] H. An, Y. Du, T. Wang, C. Wang, W. Hao, J. Zhang, Rare Met. 27 (2008) 243–250.
[6] X.P. Lin, T. Huang, F.Q. Huang, W.D. Wang, J.L. Shi, J. Phys. Chem. B 110 (2006) 24629–24634.
[7] W. Wang, F. Huang, X. Lin, Scr. Mater. 56 (2007) 669–672.
[8] W. Wang, F. Huang, X. Lin, J. Yang, Catal. Commun. 9 (2008) 8–12.
[9] C.H. Wang, C.L. Shao, Y.C. Liu, L. Zhang, Scr. Mater. 59 (2008) 332–335.
[10] J. Zhang, F. Shi, J. Lin, D. Chen, J. Goa, Z. Huang, X. Ding, C. Tang, Chem. Mater. 20 (2008) 2937–2941.
[11] S. Shenawi-Khalil, V. Uvarov, Y. Kritsman, E. Menes, I. Popov, Y. Sasson, Catal. Commun. 21 (2011) 1136–1141.
[12] Y.C. Seung, J.K. Yong, H.J. Jung, K.C. Ashok, J. Dongwoon, I.L. Wan, J. Catal. 262 (2009) 144–149.
[13] S. Shamaila, A.K.L. Sajjad, F. Chen, J. Zhang, J. Colloid Interface Sci. 356 (2011) 465–472.
[14] Y. Li, J. Wang, H. Yao, L. Dang, Z. Li, Catal. Commun. 12 (2011) 660–664.
[15] X.F. Chang, Y. Gang, J. Haung, Z. Li, S.F. Zhu, P.F. Yu, C. Cheng, S.B. Deng, G.B. Ji, Catal. Today 153 (2010) 193–199.
[16] H.F. Chang, B.B. Huang, Y. Dai, X.Y. Qin, X.Y. Zhang, Langmuir 26 (2010) 6618–6624.
[17] X. Zhang, L.Z. Zhang, T.F. Xie, D.J. Wang, J. Phys. Chem. C 113 (2009) 7371–7378.
[18] L. Zhang, W.Z. Wang, L. Zhou, M. Shang, S.M. Sun, Appl. Catal. B: Environ. 90 (2009) 458–462.
[19] S. Shenawi-Khalil, V. Uvarov, E. Menes, I. Popov, Y. Sasson, Appl. Catal. A: Gen. 413-414 (2012) 1–9.
[20] S. Horikoshi, F. Hojo, H. Hikaka, N. Serpone, Environ. Sci. Technol. 38 (2004) 2198–2208.
[21] C. Goia, E. Matijevic, D.V. Goia, J. Mater. Res. 20 (2005) 1507–1514.
[22] G.F. Hüttig, T. Tsuji, B. Steiner, Z. Anorg, Allg. Chem. 200 (1931) 74–81.
[23] C. Frondel, Am. Mineral. 28 (1943) 521–535.
[24] F.H. Chung, J. Appl. Crystallogr. 7 (1974) 519–525.
[25] V. Uvarov, I. Popov, Mater. Charact. 58 (2007) 883–891.
[26] J. Pramăna, J. Phys. 28 (1987) 293–297.
[27] C.L. Yu, J.C. Yu, C.F. Fan, H.R. Wen, S.J. Hu, Mater. Sci. Eng. B 166 (2010) 213–219.
[28] K.I. Ishibashi, A. Fujishima, T. Watanabe, K. Hashimoto, J. Photochem. Photobiol. A: Chem. 134 (2000) 139–142.
[29] J. Li, W. Ma, Y. Huang, X. Tao, J. Zhao, Y. Xu, Appl. Catal. B: Environ. 48 (2004) 17–24.
[30] H. Fu, C. Pan, W. Yao, Y. Zhu, J. Phys. Chem. B 109 (2005) 22432–22439.
[31] S. Kim, W. Choi, Environ. Sci. Technol. 36 (2002) 2019–2025.
[32] Y. Oosawa, M. Grätzel, J. Chem. Soc., Faraday Trans. 1 84 (1988) 197–205.
[33] S.H. Yoon, J.H. Lee, Environ. Sci. Technol. 39 (2005) 9695–9701.
[34] A.H. Nethercot Jr., Phys. Rev. Lett. 33 (1974) 1088–1091.
[35] C. Karunakaran, P. Anilkumar, J. Mol. Catal. A 265 (2007) 153–158.